Topology optimization for maximizing linear buckling load based on level set method

Naoyuki ISHIDA*, Tsuguo KONDOH*, Kozo FURUTA*, Hao LI*, Kazuhiro IZUI*
and Shinji NISHIWAKI*

* Department of Mechanical Engineering and Science, Kyoto University
Kyodaikatsura, Nishikyo-ku, Kyoto, 615-8540, Japan
E-mail: ishida.naoyuki.23m@st.kyoto-u.ac.jp

Abstract

Stability and buckling have attracted extensive attention in the design of structural elements, especially in the design of thin–walled structures since they may naturally have poor stability and be prone to buckling failure. This paper proposes a level-set based topology optimization (TO) method that can maximize the lowest linear buckling load under a mean compliance constraint. First, we conduct the linearized buckling analysis and formulate the optimum design problem. Second, we derive the design sensitivity and revisit the reaction–diffusion equation-based level-set topology optimization. Finally, we solve several two-dimensional benchmark problems and the design results are presented to validate the proposed method.

Keywords : Topology optimization, Level–set method, Maximizing linear buckling load, Eigenvalue problem, Linearized buckling analysis, Sensitivity analysis

1. Introduction

Structural stability is of critical importance in the design of mechanical products, especially in the design of thin–walled structures. The buckling load obtained by the linearized buckling analysis is an efficient approach to approximately estimate the structural stability performance, although the buckling load analysis does not provide a perfectly accurate buckling load. In short, the maximization of the buckling load based on the linearized buckling analysis can be used to enhance the structural stability.

Structural optimization techniques have been widely used to find optimal structures with a higher stability (Vanderplaats, 1982; Nishiwaki et al., 2013). Structural optimization can be broadly classified into three categories: size optimization, shape optimization, and topology optimization (Bendsøe and Kikuchi, 1988; Allaire et al., 1997). Among them, topology optimization (TO) is known as the most flexible design method that allows topological changes such that one can obtain a free-form conceptual design in a given design space.

The topology optimization problem is essentially an ill-posed problem since there are possibilities to include an infinite number of discontinuities in the design domain due to the introduction of the characteristic function. An appropriate mathematical method should be introduced to overcome this critical problem. The homogenization design method was first proposed by Bendsøe and Kikuchi (1988), where the homogenization method is used for the relaxation of the design domain. The density approach, also known as the SIMP method, is one of the most popular methods that uses the penalized density for convexifying the design domain (Bendsøe,1989). And phase field methods where the phase field can be evolved using a time-dependent PDE were proposed (Burger and Stainko, 2006)(Wang and Wang, 2004)(Takezawa et al., 2010).

The level-set method (LSM) is an alternative method and has become popular in recent decades. LSM has the ability to describe clear boundaries between different phases, meaning that there are no gray scale elements existing during the optimization process. Allaire et al. (2002; 2004) and Wang et al. (2003) independently proposed a Hamilton-Jacobi equation-based LSM for varying the boundary according to the shape sensitivity information. Yamada et al. (2010) proposed the reaction–diffusion equation-based LSM which uses the Ersatz material approach.

As has been discussed above, it is essential to consider the structural stability in addition to the stiffness when designing mechanical structures. Especially, the thin wall structures are prone to buckling failure, and deform largely because of the low second moment of area.

Several relevant research works can be found in the literature. Kanno et al. (2001) proposed a size optimization method for the truss structure design considering the linearized buckling load as an objective function. Yamada et al. (2013) studied the influence of stability requirements by considering the geometric nonlinearity using the MPS (Moving Particle Semi-implicit) method. They found that the design results can avoid unstable behavior in response to design loads. However, the buckling analysis was not performed in the formulation. Unlike their study, Neves et al. (1995; 2002) presented a homogenization design method to design a periodic microstructure which can minimize the mean compliance under a linear buckling load constraint. Recently, Gao and Ma (2015) adopted the SIMP method for the optimization of a continuum structure. In Dunning et al. (2016), aiming at the need for a large number of linear buckling modes, they showed how several features of the block Jacobi conjugate gradient eigenvalue method, such as optimal shift estimates, adaptive eigenvector tolerances, the reuse of eigenvectors, and multiple shifts, can be utilized to compute a large number of buckling eigenmodes in an efficient and robust way. Yi et al. (2019) have proposed a similar method with Helmholtz regularization for lattice structure. Ferrari and Sigmund (2019) presented several features of optimization for improving the buckling performance. It can be said that some achievements have been made by applying those shape and topology optimization techniques.

As has been briefly discussed above, most of the previous works focused on the influence of stability requirements, by means of considering a constraint on the linearized fundamental buckling load factor, in a minimum compliance TO problem. Unlike these works, we formulate the optimum design problem by maximizing the linearized buckling load, instead of solving a minimum compliance problem, in order to maximize the structural stability. An inequality constraint of the mean compliance is introduced to avoid the physically unreasonable local optima. The reaction-diffusion equation-based level-set method is constructed. The linearized buckling analysis is conducted by using the finite element method implemented in a COMSOL with Matlab environment. The design sensitivity derived, based on the continuous adjoint method, is verified by the finite difference method. Several two-dimensional numerical examples are presented to support the effectiveness of the proposed methodology.

This paper is organized as follows. Section 2 describes the formulation about linearized buckling analysis. Section 3 explains the formulation of the level set-based topology optimization. In Section 4, we derive the sensitivity analysis for the buckling load maximization problem and in Section 5 we show the algorithm to obtain the optimal solution. In Section 6, some numerical examples and evaluation are shown. The conclusion is provided in Section 7.

2. Linearized Buckling Analysis

In this section, we will first describe the formulation of the linearized buckling analysis in Section 2.1. We then formulate in Section 2.2 the optimum design problem.

2.1. Formulation

Let us consider a mechanical system and we assume an external force to be applied on a portion of its boundary. Then stiffness of the structure will be changed due to: (1) the deformation of the structure, or (2) the generation of stress inside the members (Washidu, 1983). Using the linearized buckling analysis, we can compute the approximate value of buckling load based only on the linear stiffness and geometric stiffness without considering that the structure deforms with an increasing load. Then, the stiffness of the entire structure can be expressed by the so-called tangential stiffness matrix $\mathbf{K_T}$, as follows:

$$\mathbf{K_T} = \mathbf{K_L} + \mathbf{K_G}\left(\mathbf{q}\right), \tag{1}$$

where $\mathbf{K_L}$ is the linear stiffness matrix, and $\mathbf{K_G}$ is the geometric stiffness matrix which is a function of the internal force vector $\mathbf{q}$. By assuming the linearity to the internal stress, the tangential stiffness matrix can be approximated as follows:

$$\begin{aligned}\mathbf{K_T} &= \mathbf{K_L} + \mathbf{K_G}\left(\lambda\mathbf{q_0}\right) \\ &\approx \mathbf{K_L} + \lambda\mathbf{K_G}\left(\mathbf{q_0}\right),\end{aligned} \tag{2}$$

where $\mathbf{q}_0$ is the internal stress vector when the unit load is applied. The critical point is where the tangential stiffness matrix $\mathbf{K}_T$ becomes singular, called the buckling point, and the linear buckling load coefficient λ is calculated based on the minimum eigenvalue of the following general eigenvalue problem (Zienkiewicz and Tayror, 2000).

$$[\mathbf{K}_L + \lambda_m \mathbf{K}_G (\mathbf{q}_0)] \, \mathbf{\Phi}_m = 0, \tag{3}$$

where λ_m denotes the m-th eigenvalue and $\mathbf{\Phi}_m$ denotes the m-th mode shape. We discuss the $\mathbf{K}_L$ and $\mathbf{K}_G$ in the two-dimensional case (Watanabe, 2005). When the domain Ω is discretized into a finite number of elements, the domain integral is as follows:

$$\int_\Omega \mathrm{d}\Omega = \sum_e^n \int_{\Omega_e} \mathrm{d}\Omega. \tag{4}$$

We follow the lead of Watanabe (2005), and define $[\mathbf{Z}_1]$ and $[\mathbf{Z}_2]$, as follows:

$$[\mathbf{Z}_1] = \begin{bmatrix} 1 + \dfrac{\partial u_1}{\partial X_1} & 0 & \dfrac{\partial u_2}{\partial X_1} & 0 \\ 0 & \dfrac{\partial u_1}{\partial X_2} & 0 & 1 + \dfrac{\partial u_2}{\partial X_2} \\ \dfrac{\partial u_1}{\partial X_2} & 1 + \dfrac{\partial u_1}{\partial X_1} & \dfrac{\partial u_2}{\partial X_2} & \dfrac{\partial u_2}{\partial X_2} \end{bmatrix} \tag{5}$$

$$[\mathbf{Z}_2] = \begin{bmatrix} \dfrac{\partial N^1}{\partial X_1} & 0 & \cdots & \dfrac{\partial N^n}{\partial X_1} & 0 \\ \dfrac{\partial N^1}{\partial X_2} & 0 & \cdots & \dfrac{\partial N^n}{\partial X_2} & 0 \\ 0 & \dfrac{\partial N^1}{\partial X_1} & \cdots & 0 & \dfrac{\partial N^n}{\partial X_1} \\ 0 & \dfrac{\partial N^1}{\partial X_2} & \cdots & 0 & \dfrac{\partial N^n}{\partial X_2} \end{bmatrix}, \tag{6}$$

where N^i is the shape function, u_i is the displacement and X_i is the basis vector. The green strain tensor due to virtual displacement δE_{ij} can be expressed as follows:

$$\delta E_{ij} = \frac{1}{2} \left(\frac{\partial \delta u_i}{\partial X_j} + \frac{\partial \delta u_j}{\partial X_i} + \frac{\partial \delta u_k}{\partial X_i} \frac{\partial u_k}{\partial X_j} + \frac{\partial u_k}{\partial X_i} \frac{\partial \delta u_k}{\partial X_j} \right), \tag{7}$$

where δu_i is virtual displacement. Then the green strain tensor due to virtual displacement $\delta \mathbf{E}$ can be discretized as follows:

$$\begin{aligned} \{\delta \mathbf{E}\} &= [\mathbf{Z}_1] \left\{ \begin{array}{c} \dfrac{\partial \delta u_1}{\partial X_1} \\ \dfrac{\partial \delta u_1}{\partial X_2} \\ \dfrac{\partial \delta u_2}{\partial X_1} \\ \dfrac{\partial \delta u_2}{\partial X_2} \end{array} \right\} \\ &= [\mathbf{Z}_1] [\mathbf{Z}_2] \{\delta \mathbf{u}^n\} \\ &= [\mathbf{B}] \{\delta \mathbf{u}^n\}, \end{aligned} \tag{8}$$

where $\{\delta \mathbf{u}^n\}$ is the virtual displacement vector and $[\mathbf{B}] = [\mathbf{Z}_1][\mathbf{Z}_2]$. Also, if the constituent matrix is $[\mathbf{D}]$, the linear stiffness matrix $\mathbf{K}_L$ can be expressed as the following equation:

$$\mathbf{K}_L = \sum_e \left[\int_{\Omega_e} [\mathbf{B}]^T [\mathbf{D}] [\mathbf{B}] \mathrm{d}\Omega \right]. \tag{9}$$

Similarly, the geometric stiffness matrix $\mathbf{K}_G$ can be expressed by the following equation:

$$\mathbf{K}_G = \sum_e \left[\iint_{\Omega_e} [\mathbf{Z}_2]^T \left[\sum_{(0)} \right] [\mathbf{Z}_2] \, d\Omega \right], \tag{10}$$

where we define S_{ij} as the stress, and the matrix is defined as follows:

$$\left[\sum_{(0)} \right] = \begin{bmatrix} [\mathbf{S}] & \mathbf{0} \\ \mathbf{0} & [\mathbf{S}] \end{bmatrix} \tag{11}$$

$$[\mathbf{S}] = \begin{bmatrix} S_{11} & S_{12} \\ S_{21} & S_{22} \end{bmatrix}. \tag{12}$$

2.2. Optimum design problem

Here we formulate the optimum design problem. Considering a fixed design domain $\Omega_D \subset \mathbb{R}^d (d = 2 \text{ or } 3)$, we intend to find the optimal topological configuration which can maximize the buckling load under a volume constraint and a mean compliance constraint. A fixed wall boundary condition is imposed on a portion of boundary Γ_{Ω_D} and a unit surface traction is applied on the boundary Γ_{Ω_N}. The mathematical optimization model can be then formulated as follows:

$$\inf_{\chi_\phi \in \mathcal{X}} J(\Omega) = -\lambda_1 \tag{13}$$

$$\text{s.t.} \quad \mathbf{K}_L \{u_n\} = f \qquad \qquad \text{in} \quad \Omega_D \tag{14}$$

$$\mathbf{u}(\Gamma_D) = 0 \qquad \qquad \text{on} \quad \Gamma_D \tag{15}$$

$$\mathbf{f}(\Gamma_N) = \bar{\mathbf{f}} \qquad \qquad \text{on} \quad \Gamma_N \tag{16}$$

$$|\mathbf{K}_L + \lambda_m \mathbf{K}_G(\{u_n\})| = 0 \qquad \qquad \text{in} \quad \Omega_D \tag{17}$$

$$(\mathbf{K}_L + \lambda_m \mathbf{K}_G)\mathbf{\Phi}_m = 0 \qquad \qquad \text{in} \quad \Omega_D \tag{18}$$

$$\mathbf{K}_L = \sum_e \left[\iint_{\Omega_e} [\mathbf{B}]^T [\mathbf{D}] [\mathbf{B}] d\Omega \right] \tag{19}$$

$$\mathbf{K}_G = \sum_e \left[\iint_{\Omega_e} [\mathbf{Z}_2]^T \left[\sum_{(0)} \right] (\{u_n\}) [\mathbf{Z}_2] \right] \tag{20}$$

$$G(\phi) = \int_{\Omega_D} \chi_\phi \, d\Omega - \bar{V} \le 0 \tag{21}$$

$$C(u, \phi) = \int_{\Gamma_N} fu \, d\Gamma - \bar{C} \le 0, \tag{22}$$

where λ_1 is the lowest eigenvalue obtained by Eq. (17). $\bar{\mathbf{f}}$ is the unit load vector, and $\mathbf{\Phi}_m$ is the discretized mode shape corresponding to λ_m. In addition, $\bar{V}$ is the maximum allowed volume of the material, $\bar{C}$ is the upper bound of the mean compliance and $\{\mathbf{u}_n\}$ is the discretized displacement vector when a unit load is applied.

The linear buckling load is computed by Eq. (18) and λ_1 can be rewritten as follows:

$$\lambda_1 = -\frac{\mathbf{\Phi}_1 \mathbf{K}_L \mathbf{\Phi}_1}{\mathbf{\Phi}_1 \mathbf{K}_G \mathbf{\Phi}_1}. \tag{23}$$

Eq. (23) is then normalized as follows:

$$\mathbf{\Phi}_1 \mathbf{K}_G \mathbf{\Phi}_1 = -1. \tag{24}$$

The above equation implies that λ_1 is equivalent to the linear stiffness modal energy. In other words, the optimum design problem of maximizing the linear buckling load is equivalent to that of maximizing the value of $\mathbf{\Phi}_1 \mathbf{K}_L \mathbf{\Phi}_1$, and this leads to the maximization of the linear stiffness modal energy. However, we may observe some structures that have isolated sub-structures in some portion as shown in Section 6.3. This can be problematic since they provide a low static stiffness. Such optimal structures are not practically useful from an engineering perspective.

In order to overcome the above-mentioned problem, we set an additional constraint to ensure that the mean compliance is not larger than a given value $\overline{C}$. Indeed, such mean compliance implementation is necessary for obtaining the realistic structures that do not greatly deform under the external loads.

In the context of eigenvalue problems, it is essentially not easy to obtain a reasonable optimal solution without considering any physical constraints. For example, in the work done by Allaire and Jouve (2005) where they proposed a level-set method for vibration and multiple loads structural optimization, they reported that the role of a heavy tip mass is to produce an optimal shape which is more robust and closer to the compliance optimal shape. The similar effect can be achieved by the introduction of a mean compliance constraint. Besides, Andreassen and Jensen (2014) solved a complex eigenvalue problem with a prescribed wave frequency, and they pointed out that most pure high damping materials exhibit a stiffness that is too low for practical application, while high stiffness materials have low damping capabilities. The observations motivated them to add the mean compliance as a constraint in their TO formulation.

3. Reaction–diffusion Equation-based Topology Optimization

3.1. Level set-based boundary expression

Here we overview the basic idea of the level-set based topology optimization method. Let us consider a computational domain denoted as $D \subset \mathbb{R}^d$. A solid phase is defined as a subdomain $\Omega \subseteq D$. The void phase is then the complementary domain as $D \backslash \Omega$. The solid and void phases are divided by the boundary $\partial \Omega$. Now we introduce an implicit level set function with a positive value in the solid domain, zero value on the boundary and a negative value in the void domain, as follows:

$$
\begin{cases}
\phi(\mathbf{x}) < 0 & \text{if } \mathbf{x} \in \Omega \\
\phi(\mathbf{x}) = 0 & \text{if } \mathbf{x} \in \partial \Omega \\
\phi(\mathbf{x}) > 0 & \text{if } \mathbf{x} \in D \backslash \Omega
\end{cases}
\tag{25}
$$

3.2. Interpolation of material property

Using a smoothed Heaviside function H, the characteristic function χ_ϕ is obtained based on the level-set function as follows:

$$
\chi_\phi \simeq H(\phi) = \begin{cases}
0 & (\phi < -w) \\
\dfrac{1}{2} + \dfrac{\phi}{w}\left[\dfrac{15}{16} - \dfrac{\phi^2}{w^2}\left(\dfrac{5}{8} - \dfrac{3}{16}\dfrac{\phi^2}{w^2}\right)\right] & (-w < \phi < w) \\
1 & (w < \phi),
\end{cases}
\tag{26}
$$

where w is the transition width of the continuous function $H(\phi)$ and we set $w = 0.5$ in this paper. Then, the Young's modulus can be interpolated using a linear scheme as follows:

$$
E_{\chi_\phi} = \mathrm{E}_0\left(\chi_\phi + \mathrm{d}_\mathrm{E}\left(1 - \chi_\phi\right)\right),
\tag{27}
$$

where E_0 is the Young's modulus of the solid material. In this paper, we set $E_0 = 6.9 \times 10^9$ Pa, and $d_\mathrm{E} = 1 \times 10^{-3}$ for the weak material (void domain). The Poisson's ratio is set to 0.3.

3.3. Level-set evolution equation

In this paper, we follow the lead of Yamada et al. (2010). We assume that a level-set function is an implicit function of a fictitious time t. The level-set function is evolved using the reaction–diffusion equation (RDE). With this level-set evolution equation, it has been proved that the Lagrangian can decrease with the fictitious time monotonically (Li et al., 2021). Thus, the RDE is defined as follows:

$$
\frac{\partial \phi(\mathbf{x}, t)}{\partial t} = -\left(\tilde{C}J' - \tau\nabla^2\phi\right),
\tag{28}
$$

where J' is the design sensitivity which will be discussed in Section 4. τ is the regularization parameter. $\tilde{C}$ is the normalizer which is defined as follows:

$$\tilde{C} = \frac{r \int_{\Omega_D} d\Omega}{\int_{\Omega_D} |J'| \, d\Omega}. \tag{29}$$

The optimization problem described by the reaction equation is an ill-posed problem. Thus, it is regularized by an additional diffusive term, which is used to guarantee the smoothness of the level-set function. The value of the level-set function should be bounded in the range of $[-1, 1]$. This constraint is to ensure that the effect of the regularization term is approximately constant around the boundaries.

4. Sensitivity analysis

We replace the above constrained optimization problem (cf. Section 2.2) with an unconstrained problem using the Lagrange method. The Lagrangian is formulated as follows:

$$
\begin{aligned}
\mathscr{L}(\phi) &:= J(\phi) + \mu_g G(\phi) + \mu_c C(\mathbf{u}, \phi) + \mathbf{u}'(\mathbf{K}_L \mathbf{u} - \mathbf{f}) \\
&= -\lambda_1 + \mu_g \left(\int_{\Omega_D} \chi_\phi \, d\Omega - \overline{V} \right) + \mu_c \left(\int_{\Gamma_N} \mathrm{fu} \, d\Gamma - \overline{C} \right) + \mathbf{u}'(\mathbf{K}_L \mathbf{u} - \mathbf{f}),
\end{aligned} \tag{30}
$$

where $\mathscr{L}$ is the Lagrangian, μ_g is the Lagrange multiplier with association to the volume constraint, μ_c is the same to the mean compliance constraint, and $\mathbf{u}'$ is the adjoint variable. The sensitivity of the buckling load maximization problem is derived as follows:

$$
\begin{aligned}
J' &= \frac{\partial \mathscr{L}}{\partial \chi_\phi} \\
&= \frac{1}{\boldsymbol{\Phi}_1^T \mathbf{K}_G \boldsymbol{\Phi}_1} \left(-\boldsymbol{\Phi}_1^T \frac{\partial \mathbf{K}_L}{\partial \chi_\phi} \boldsymbol{\Phi}_1 + \lambda_1 \boldsymbol{\Phi}_1^T \frac{\partial \mathbf{K}_G}{\partial \chi_\phi} \boldsymbol{\Phi}_1 \right) + \mathbf{u}'^T \frac{\partial \mathbf{K}_L}{\partial \chi_\phi} \mathbf{u} + \mu_g + \mu_c \mathbf{u} \, [\mathbf{B}] \, [\mathbf{D}] \, [\mathbf{B}] \, \mathbf{u}.
\end{aligned} \tag{31}
$$

And the adjoint variable can be computed by solving the following adjoint equation:

$$
\mathbf{K}_L \mathbf{u}' + \lambda_1 \frac{\boldsymbol{\Phi}_1^T \frac{\partial \mathbf{K}_G}{\partial \mathbf{u}} \boldsymbol{\Phi}_1}{\boldsymbol{\Phi}_1^T \mathbf{K}_G \boldsymbol{\Phi}_1} = 0. \tag{32}
$$

The details of the sensitivity analysis can be referred to in Appendix A.

5. Optimization Algorithm

Fig. 1 shows the optimization flowchart. First, we initialize the level-set function ϕ. Next, the eigenvalue problem is solved using the finite element method (FEM), and the objective functional is calculated. If the objective functional does not converge, the adjoint equation will be solved. Then the design sensitivity is calculated and the level-set function ϕ is updated by solving RDE. The aforementioned workload will be terminated until the convergence criteria (see Eq. (33)) is satisfied for 5 iterative steps in a sequence.

$$\left| J_i - J_{i-1} \right| < \varepsilon. \tag{33}$$

6. Numerical examples
6.1. Design problem setting

In this section, we will present three different test cases #1, #2 and #3. The design model for test case #1 is shown in Fig. 2 . The design domain is a rectangle with a dimension of $10 \, \mathrm{m} \times 1 \, \mathrm{m}$. The left end is fixed, and the right end is under a surface traction of $\mathbf{f} = [-1, 0]^T \mathrm{N} \, \mathrm{m}^{-1}$. The top and bottom surfaces are treated as free boundary. We consider two different types of boundary conditions: (i) free B.C., and (ii) fixed only in the y direction. We set the proportionality
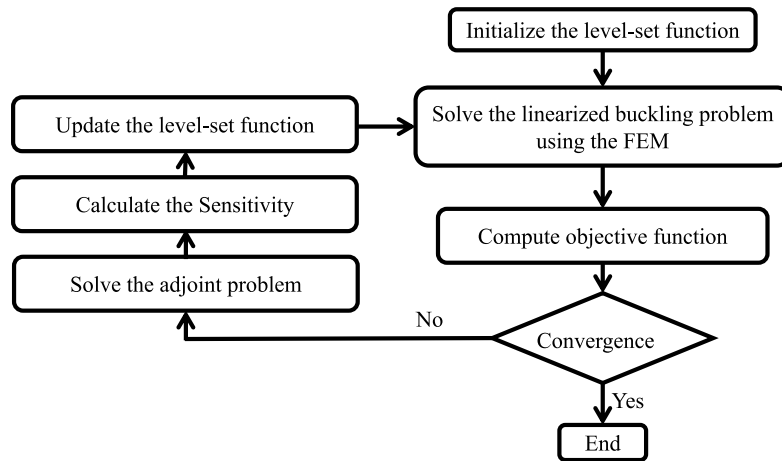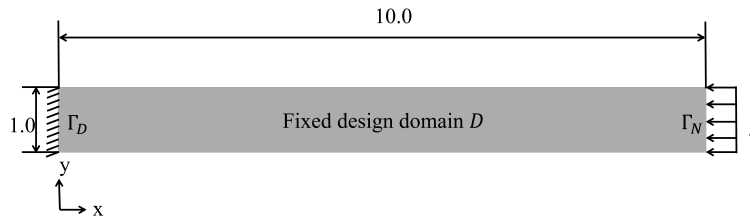
Fig. 1 Optimization flow chart.

Fig. 2 Design model for test case #1.

constant $K = 1.0$ and the characteristic length $L = 10\,\text{m}$ in the reaction-diffusion equation, Eq. (28). The maximum allowed volume fraction is set to $\overline{V} = 60\%$, and the upper bound of the stiffness is set to $\overline{C} = 1.7C_0$ where C_0 is the initial value of the mean compliance. The regularization coefficient is set to $\tau = 1.0 \times 10^{-4}$. The computational domain is discretized into 1000×100 quadrilateral elements.

The design model for test case #2 is shown in Fig. 3 for comparing the optimized result to the previous work (Ferrari et al, 2021). The fixed design domain is coated by a solid domain with thickness of $0.04\,\text{m}$, clamped at the base. The surface traction is applied at the left end with $\mathbf{f} = [1,0]^T\ \text{N}\,\text{m}^{-1}$. We set the characteristic length to $L = 1.0\,\text{m}$, the upper bound of stiffness to $\overline{C} = 1.6C_0$ and the upper bound of volume to $\overline{V} = 50\%$. The other coefficients are set to the same as in test case #1. The computational domain is discretized into 7600 quadrilateral elements.

The design model for test case #3 is shown in Fig. 4. The fixed design domain is a rectangle with a dimension of $4\,\text{m} \times 1\,\text{m}$. The lower left is fixed, the lower right is fixed only in the y direction, and the load boundary of $\mathbf{f} = [-1,0]^T\text{N}\,\text{m}^{-1}$ is applied in the lower middle. We set the characteristic length $L = 4.0\,\text{m}$ and the lower bound of stiffness $\overline{C} = 1.4C_0$. The other coefficients are set the same with test case #1. The computational domain is discretized into 400×100 quadrilateral elements.

In this paper, we initialize the fixed design domain D with solid phase. And the Q_4 isoparametric elements are used to discretize the computational domain.

6.2. Validation of numerical analysis and sensitivity

Before we start to optimize the structure, we should first validate the numerical modeling and the deduced sensitivity. In Section 6.2.1, we will compare the numerical and analytical solutions for the linearized buckling analysis. In Section 6.2.2, we will compare the deduced sensitivity with that computed using the finite difference method.

6.2.1. Linearized buckling analysis

We construct a verification model as shown in Fig. 5. Knowing the Young's modulus E_r, cross sectional area $h_r \times b_r$ ($h_r \leq b_r$), and the length l_r, the analytical solution can be found in Shibata et al. (1991).

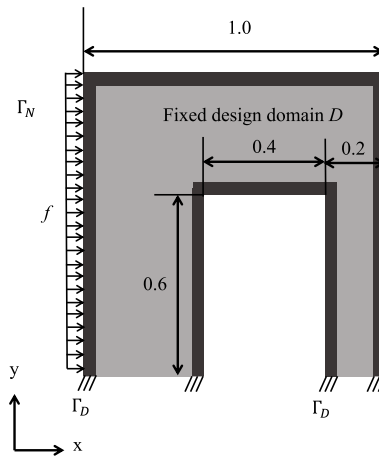For the case where the right end is set to be a free boundary:
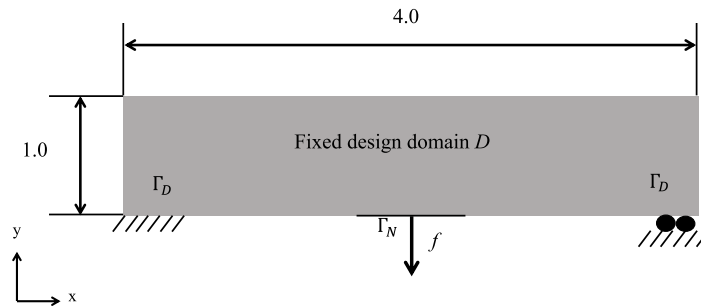
Fig. 3 Design model for test case #2.

Fig. 4 Design model for test case #3.

$$Pr_1 = \frac{\pi^2 E_r}{4 l_r^2} \frac{1}{12} b_r h_r^{\ 3} \tag{34}$$

For the case where the right end is fixed only in the *y* direction:

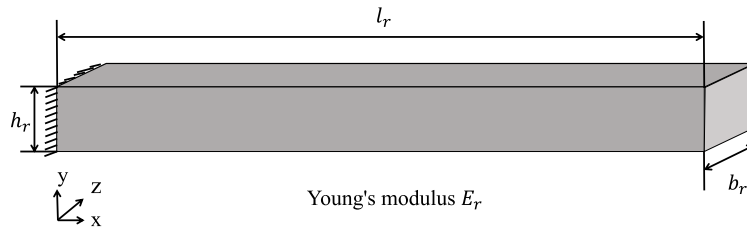$$Pr_2 = \frac{2.046 \pi^2 E_r}{l_r^2} \frac{1}{12} b_r h_r^{\ 3}. \tag{35}$$

Fig. 5 Model for the analytical solution.

For a two-dimensional case, the analytical solution is $\dfrac{Pr}{b_r}$. We set $E_r = 6.9 \times 10^9$ Pa, $l_r = 10$ m and $h_r = 10$ m. The analysis results and the numerical results on test caes #1 are summarized in Tables 1 and 2. The relative errors are less than 9.82% for both cases. Hence, the accuracy of the numerical model is validated.

Table 1 Fixed-free boundary.

Analytical solution $\mathrm{N\,m^{-1}}$	Numerical solution $\mathrm{N\,m^{-1}}$	Relative error
1.42×10^7	1.56×10^7	9.82%

Table 2 Fixed-simple support boundary.

Analytical solution $\mathrm{N\,m^{-1}}$	Numerical solution $\mathrm{N\,m^{-1}}$	Relative error
1.16×10^8	1.18×10^8	1.72%

Next, we clarify the effect of the mesh resolution on the buckling analysis accuracy. We summarize in Table 3 the buckling analysis results obtained by different element numbers in test case #1 and the relative errors compared with the analytical solution. It can be seen that the numerical errors become mesh independent when the number of elements reaches 100×1000. Therefore, we use this level of mesh resolution in the numerical examples.

Table 3 Buckling analysis result obtained by different element numbers and the relative errors compared with the analytical solution.

Element number	Linearized buckling load [$\mathrm{N\,m^{-1}}$]	Relative error
5×50	1.5603×10^7	9.88%
10×100	1.5597×10^7	9.84%
20×500	1.5595×10^7	9.83%
100×1000	1.5594×10^7	9.82%
200×5000	1.5594×10^7	9.82%

6.2.2. Design sensitivity

The sensitivity information can be computed based on the finite difference (FD) method as follows (Kishimoto, 2017):

$$\tilde{J} := \frac{(j + \delta j) - j}{|\mathrm{meas}(\Omega \backslash \Omega_\varepsilon) - \mathrm{meas}(\Omega)|}, \tag{36}$$

where δj is the amount of change in the objective functional when a small hole Ω_ϵ with a radius of $\epsilon = 0.05$ is nucleated. Fig. 6 plots the sensitivity as a function of the x-coordinate on the cut line $y = 0.3, x \in [0.1, 9.7]$. The results show that the deduced sensitivity agrees well with its FD-based counterpart.
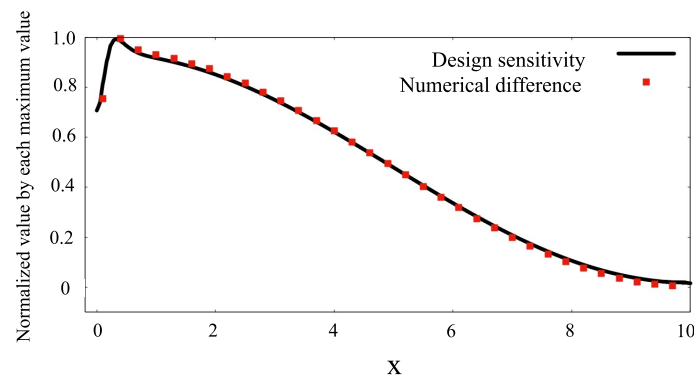
Fig. 6 Sensitivity as a function of x-coordinate on the cut line $y = 0.3, x \in [0.1, 9.7]$.

6.3. The mean compliance constraint

Here we use test case #1 to illustrate the necessity of the mean compliance constraint. First, we plot one of the optimal solutions obtained without considering a mean compliance constraint. As shown in Fig. 7, we can observe the isolated sub-structures. The optimized value of the linear buckling load is 94% of the initial value. However, such an optimal

solution makes no sense from an engineering perspective though it shows a better functional performance compared with the one shown in Fig. 10 where a mean compliance constraint is imposed.
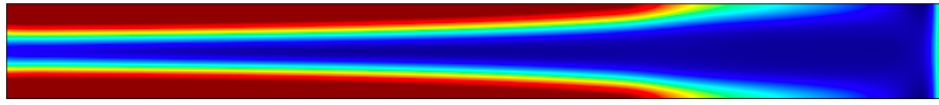

Fig. 7 The optimal solution obtained with no mean compliance constraint being applied for test case #1.

To further investigate the reasons for that, we plot the sensitivity distribution, broken down into three terms given in Eq. (31). From Figs. 8b and c, we can observe a sudden change in sensitivity value at the right side of the beam. This indeed results in a disconnection of the optimized structure.
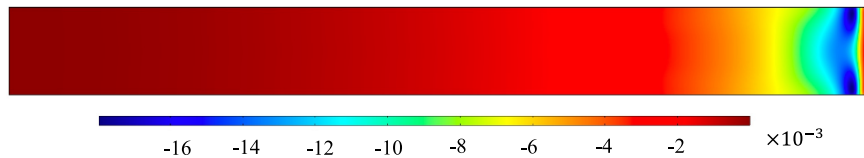
In addition, as can be observed from Fig. 8d, the sensitivity distribution at the final iterative step becomes the same as that of the obtained optimal solution so the material distribution ϕ does not change. In short, the optimization problem falls into a local solution.
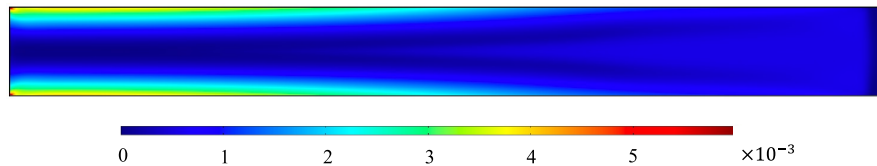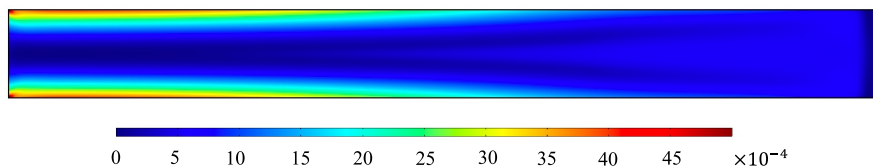

(a) The first term of sensitivity.
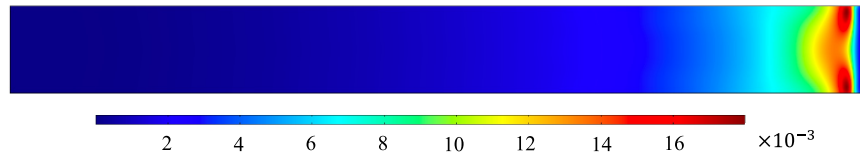
(b) The second term of sensitivity.

(c) The third term of sensitivity.

(d) Sensitivity (the sum of above all).

Fig. 8 Sensitivity distribution at the final iterative step.

6.4. Optimal structures

The obtained optimal structures of test case #1 are shown in Fig. 9. By considering the mean compliance constraint, the optimal solution becomes clear 1/0 binary structure. The material is distributed on the outside of the fixed design domain, which means two long structures support the load. The structures that have only one long structure in the middle

can be considered generically as another simple optimal structure. However, even if the cross-sectional area of each long structure is smaller than that of one long structure, the buckling load as a whole increases. It can be seen that the optimal structures of free boundary and fixed boundary in the y direction are almost the same. Next, the buckling modes are shown in Fig. 10. They transform where they meet their respective boundary conditions. At the end, we show the eigenvalue's history of the free boundary in Fig. 11. The horizontal axis is the number of iterations and the vertical axis is the eigenvalue. We plot up to the third eigenvalue. From this figure, it can be seen that there is no switching of eigenvalue in this model. The linear buckling load converges at 0.37 times the initial value. The reason why the linear buckling load decreases is the more material that exists, the stronger the structure is.
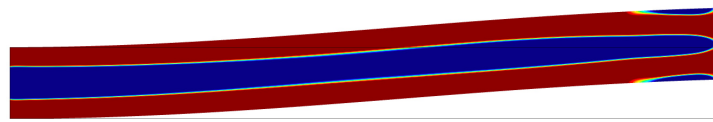

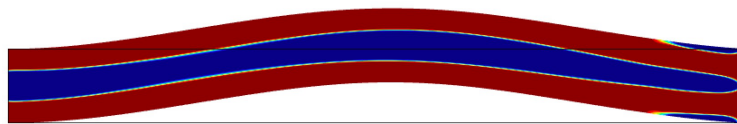(a) The free boundary condition is given at the right end.

(b) The fixed boundary condition only in the y direction is given at the right end.

Fig. 9 Optimal structures of test case #1.

(a) The free boundary condition is given at the right end.

(b) The fixed boundary condition only in the y direction is given at the right end.

Fig. 10 Deformations observed in the optimal structures of test case #1
.

The obtained optimal structures for test case #2 are shown in Fig. 12. Fig. 12a shows the solution for the mean compliance minimization problem without the buckling constraint which resembles the case in Ferrari et al. quite well. Fig. 12b shows the optimal solution for the case of maximizing the linearized buckling load under the mean compliance constraint. Although the overall configurations are largely similar with each other, one can still find several design details which are slightly different from the mean compliance minimization solution without the buckling constraint, mainly appearing in the top left portion of the design domain. To further investigate the reason behind this, we apply the body-fitted mesh to the optimal structures by using the COMSOL and conduct the buckling analysis, as shown in Fig. 13. From Figs. 13b and e, the deformations clearly show that the top left portion of the structure is prone to buckling where the slender bars are subjected to the compressible force. Moreover, the minimum principal stress in Fig. 13f is lower than that in Fig. 13c, which offers a better structural stability. We then summarize in Table 4 the linearized buckling load and the normalized mean compliance values. From the comparison results, it can be found that with the proposed method, the buckling load is 16% higher than that of the mean compliance minimization solution without the buckling constraint.
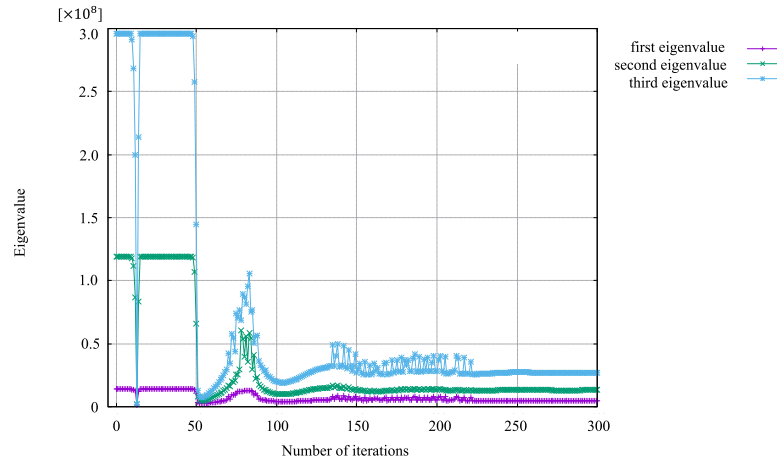
Fig. 11 Eigenvalue history of test case #1 with a free boundary condition at the right end, cf. Fig. 9a.

Furthermore, the results obtained by the proposed method are compared with those by the minimal mean compliance problem under a buckling constraint. To make this comparison fair enough, we set the lower limit of the buckling constraint to be the same as the objective value of the proposed method. The optimal solution is shown in Fig. 12c. Comparing Figs. 12b and c, it can be observed that the structures look quite similar especially at the places where the buckling failure occurs, although one can argue that there are still slight differences in the lower left portion of the design domain. This may be caused by the different update schemes of the Lagrange multipliers. It is quite common in topology optimization since one can only expect to reach local optima. On the other hand, from Table 4, it can be found that the difference between the two buckling loads is less than 0.7%, which implies that the two TO formulations are essentially equivalent with each other. From the above results, we have confirmed the effectiveness of the proposed method.

(a) Mean compliance minimization.

(b) Buckling maximization.

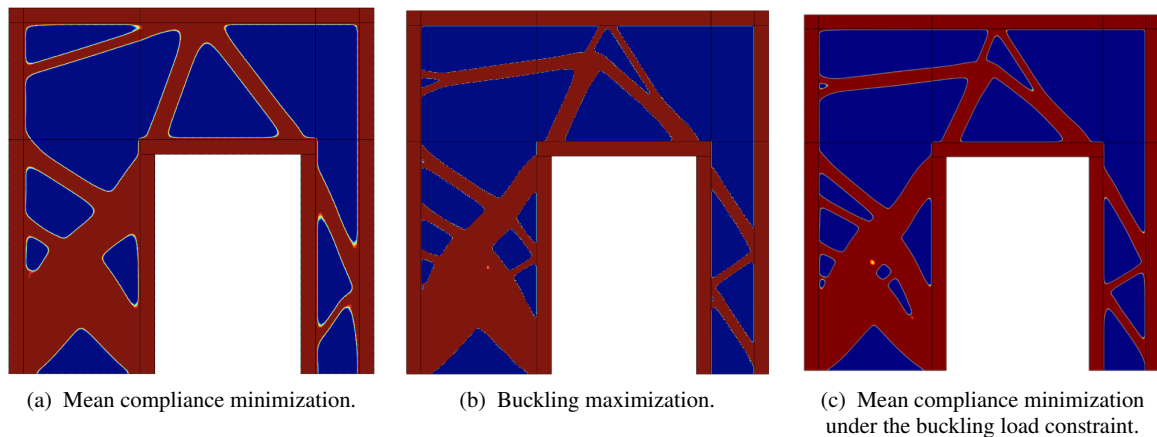(c) Mean compliance minimization under the buckling load constraint.

Fig. 12 Optimal solutions for test case #2 obtained by (a) minimizing the mean compliance, (b) maximizing the linearized buckling load under the mean compliance constraint, and (c) minimizing the mean compliance under the buckling load constraint.

Next, we show the obtained optimal structures of test case #3 in Fig.14. The structure is stable against axial force. The optimal structure is shaped to receive force along the axial direction to increase structural stability. We plot the history of up to the third eigenvalue in Fig. 15. The linear buckling load converges at 0.85 times the initial value. Although there are some unstable iteration steps, there is no switching of eigenvalue in the optimization process as before. Setting the objective function to only the lowest eigenvalue has no adverse effect in these models. As a matter of fact, there is no guarantee that these phenomena can be eliminated by applying only the mean compliance constraint. If this is the case, λ_i and $(i \geq 2)$ should be considered to fully reflect the buckling behavior, which is targeted in our future work.

(a) Mesh.   (b) Deformation.   (c) Minimum principal stress σ_{II}.

(d) Mesh.   (e) Deformation.   (f) Minimum principal stress σ_{II}.

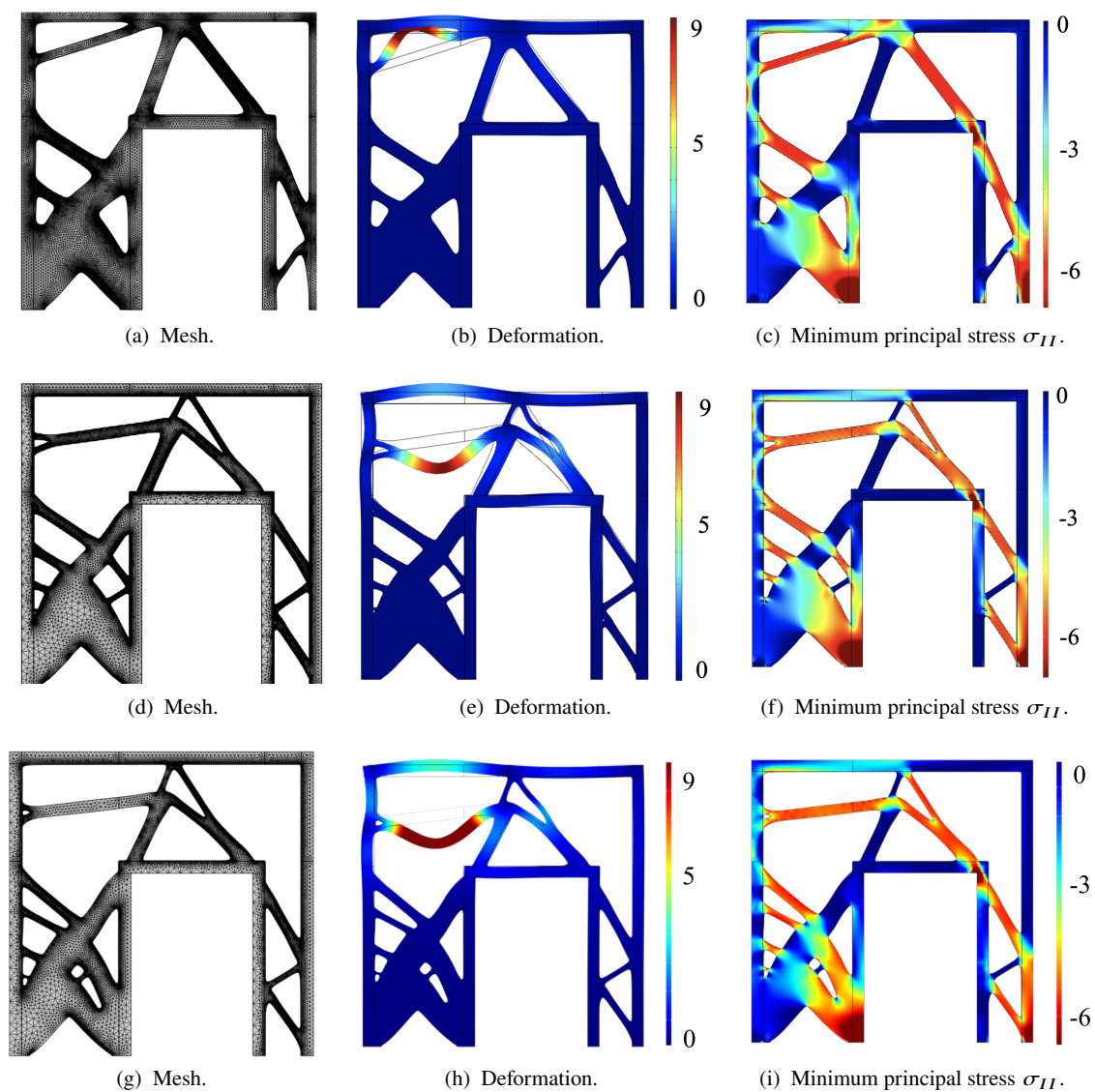(g) Mesh.   (h) Deformation.   (i) Minimum principal stress σ_{II}.

Fig. 13 Buckling analysis results obtained by the validation model using body-fitted mesh for both the mean compliance minimization solution (upper row), buckling maximization solution under the mean compliance constraint (middle row), and the mean compliance minimization solution under the buckling load constraint (lower row).

Table 4 Buckling analysis results and the normalized mean compliance values computed by the validation model using body-fitted mesh (cf.Fig. 13).

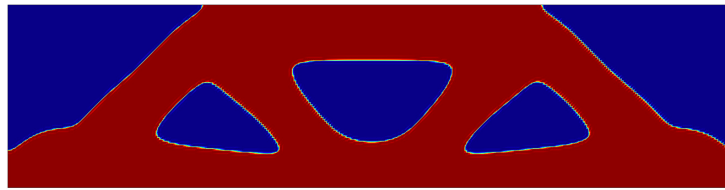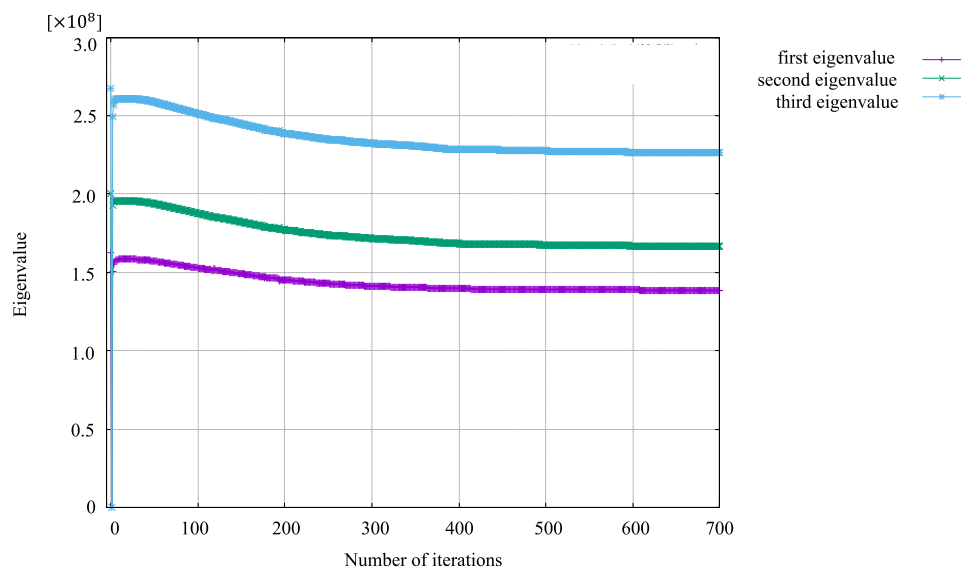|	Linearized buckling load [N m^{-1}]	Normalized mean compliance
Mean compliance minimization (cf. Fig. 12a)	2.61×10^7	1.6
Buckling maximization with mean compliance constraint (cf. Fig. 12b)	3.03×10^7	1.6
Mean compliance minimization with buckling constraint (cf. Fig. 12c)	3.05×10^7	1.6

Fig. 14 Optimal structure of test case #3.

Fig. 15 Eigenvalue history of test case #3, cf. Fig. 14.

7. Conclusion

In this paper, we constructed a level set-based topology optimization method that can maximize the lowest linear buckling load under the mean compliance constraint. The main target in this paper was to obtain high structural stability. The main findings of this work can be concluded as follows:

（１） The maximal linear buckling optimization problem was formulated. The sensitivity and adjoint equations which we derived were confirmed using the differential sensitivity.

（２） The reaction–diffusion equation-based topology optimization method was constructed. By illustrating three numerical examples, we showed the validity of the constructed algorithm.

（３） In test case #1, we showed the necessity of the mean compliance constraint. We observed the introduction of the mean compliance constraint allows us to obtain practically useful optimal structures.

（４） Test case #2 showed the difference between our method and the previous work and indicated the effectiveness of our method to maximize the linearized buckling load.

（５） We applied the proposed method to a new model setting as test case #3 and we could obtain the optimized structure.

Appendix A

Here, we describe the derivation of sensitivity in detail. First, we define the objective function j.

$$j\left(\lambda_1(\chi_\phi, \mathbf{u}(\chi_\phi))\right) = -\lambda_1, \tag{A.1}$$

where λ_1 is the real lowest eigenvalue. Next, we define the extended objective function J as follows:

$$J\left(\lambda(\chi_\phi, \mathbf{u}(\chi_\phi)); \mathbf{u}'; \mathbf{u}(\chi_\phi); \chi_\phi\right) = -\lambda_1 + \mathbf{u}'(\mathbf{K}_L \mathbf{u} - \mathbf{f}). \tag{A.2}$$

where $\mathbf{u}'$ is the Lagrange multiplier. We derive the design sensitivity $\hat{J}$ obtained by differentiating the extended objective function J with respect to the characteristic function χ_ϕ.

$$\hat{J} = \frac{\mathrm{d}J}{\mathrm{d}\chi_\phi}\left(\lambda(\chi_\phi, \mathbf{u}(\chi_\phi)); \mathbf{u}'; \mathbf{u}(\chi_\phi); \chi_\phi\right). \tag{A.3}$$

When applying the chain's rule, the above equation can be rewritten as follows:

$$\hat{J} = \frac{\partial J}{\partial \lambda_1}\frac{\partial \lambda_1}{\partial \chi_\phi} + \frac{\partial J}{\partial \lambda_1}\frac{\partial \lambda_1}{\partial \mathbf{u}}\frac{\partial \mathbf{u}}{\partial \chi_\phi} + \frac{\partial J}{\partial \mathbf{u}}\frac{\partial \mathbf{u}}{\partial \chi_\phi} + \frac{\partial J}{\partial \chi_\phi} \tag{A.4}$$

$$= \frac{\partial J}{\partial \lambda_1}\frac{\partial \lambda_1}{\partial \chi_\phi} + \left(\frac{\partial J}{\partial \lambda_1}\frac{\partial \lambda_1}{\partial \mathbf{u}} + \frac{\partial J}{\partial \mathbf{u}}\right)\frac{\partial \mathbf{u}}{\partial \chi_\phi} + \frac{\partial J}{\partial \chi_\phi}. \tag{A.5}$$

The contingent field $\mathbf{u}'$ is defined as follows so that the second term on the right hand side of the above equation yields to zero.

$$\mathbf{K}_L \mathbf{u}' + \lambda_1 \frac{\mathbf{\Phi}_1^T \dfrac{\partial \mathbf{K}_G}{\partial \mathbf{u}} \mathbf{\Phi}_1}{\mathbf{\Phi}_1^T \mathbf{K}_G \mathbf{\Phi}_1} = 0. \tag{A.6}$$

We describe $\mathbf{\Phi}_1^T \dfrac{\partial \mathbf{K}_G}{\partial \mathbf{u}^{(n)}} \mathbf{\Phi}_1$ in Eq. (A.6) in detail. $\{\mathbf{u}^{(n)}\}$ can be expanded as follows:

$$\{\mathbf{u}^{(n)}\} = [1, 0, 1, 0, ..., 1, 0]^T\{u_1^{(n)}\} + [0, 1, 0, 1, ..., 0, 1]^T\{u_2^{(n)}\} \tag{A.7}$$

Thus, $\mathbf{\Phi}_1^T \dfrac{\partial \mathbf{K}_G}{\partial \mathbf{u}^{(n)}} \mathbf{\Phi}_1$ can be expanded as follows:

$$
\frac{\partial(\mathbf{\Phi}^T \mathbf{K}_G \mathbf{\Phi})}{\partial \mathbf{u}^{(n)}} = \begin{bmatrix} \dfrac{\partial(\mathbf{\Phi}^T \mathbf{K}_G \mathbf{\Phi})}{\partial u_1^{(n)}} \\[2mm] \dfrac{\partial(\mathbf{\Phi}^T \mathbf{K}_G \mathbf{\Phi})}{\partial u_2^{(n)}} \end{bmatrix}
$$

$$
= \begin{bmatrix} \sum_e \left[\{\mathbf{\Phi}\}^T \int_{\Omega_e} [\mathbf{Z}_2] \dfrac{\partial}{\partial u_1^{(n)}} \begin{bmatrix} [\mathbf{S}]\{\mathbf{u}^{(n)}\} & 0 \\ 0 & [\mathbf{S}]\{\mathbf{u}^{(n)}\} \end{bmatrix} [\mathbf{Z}_2] d\Omega\{\mathbf{\Phi}\}\right] \\[4mm] \sum_e \left[\{\mathbf{\Phi}\}^T \int_{\Omega_e} [\mathbf{Z}_2] \dfrac{\partial}{\partial u_2^{(n)}} \begin{bmatrix} [\mathbf{S}]\{\mathbf{u}^{(n)}\} & 0 \\ 0 & [\mathbf{S}]\{\mathbf{u}^{(n)}\} \end{bmatrix} [\mathbf{Z}_2] d\Omega\{\mathbf{\Phi}\}\right] \end{bmatrix}
$$

$$
= \begin{bmatrix} \sum_e \left[\{\mathbf{\Phi}\}^T \int_{\Omega_e} [\mathbf{Z}_2] \begin{bmatrix} [\mathbf{S}][1, 0, .., 1, 0]^T & 0 \\ 0 & [\mathbf{S}][1, 0, .., 1, 0]^T \end{bmatrix} [\mathbf{Z}_2] d\Omega\{\mathbf{\Phi}\}\right] \\[4mm] \sum_e \left[\{\mathbf{\Phi}\}^T \int_{\Omega_e} [\mathbf{Z}_2] \begin{bmatrix} [\mathbf{S}][0, 1, .., 0, 1]^T & 0 \\ 0 & [\mathbf{S}][0, 1, .., 0, 1]^T \end{bmatrix} [\mathbf{Z}_2] d\Omega\{\mathbf{\Phi}\}\right] \end{bmatrix}. \tag{A.8}
$$

References

Allaire, G., Bonnetier, E., Francfort, G., and Jouve, F., Shape optimization by the homogenization method. Numerische Mathematik, Vol.76, No.1 (1997), pp.27-68.

Allaire, G., and Jouve, F.,A level-set method for vibration and multiple loads structural optimization. Computer Methods in Applied Mechanics and Engineering, Vol.194, No.30–33 (2005), pp.3269-3290.

Allaire, G., Jouve, F., and Toader, A. M., A level-set method for shape optimization. Comptes Rendus Mathematique, Vol. 334, No.12 (2002), pp.1125-1130.

Allaire, G., Jouve, F., and Toader, A. M., Structural optimization using sensitivity analysis and a level-set method. Journal of Computational Physics, Vol.194, No.1 (2004), pp.363-393.

Andreassen, E., and Jensen, J. S., Topology optimization of periodic microstructures for enhanced dynamic properties of viscoelastic composite materials, Structural and Multidisciplinary Optimization, Vol.49, No.5 (2014), pp.695-705.

Burger, M., and Stainko, R., Phase-field relaxation of topology optimization with local stress constraints. Society for Industrial and Applied Mathematics, Vol.45, No.4 (2006), pp.1447-1466.

Bendsøe, M. P., and Kikuchi, N., Generating optimal topologies in structural design using a homogenization method. Computer Methods in Applied Mechanics and Engineering, Vol.71, No.2 (1988), pp.197-224.

Bendsøe, M. P., Optimal shape design as a material distribution problem. Structural Optimization, Vol.1, No.4 (1989), pp.193-202.

Dunning, P. D., Ovtchinnikov, E., Scott, J., and Kim, H. A., Level-set topology optimization with many linear buckling constraints using an efficient and robust eigensolver. Numerical Methods in Engineering, Vol.107, No. 17 (2016), pp.1029-1053.

Ferrari, F. and Sigmund, O., Revisiting topology optimization with buckling constraints. Structural and Multidisciplinary Optimization, Vol.59, No.5 (2019), pp.1401-1415.

Ferrari, F. and Sigmund, O., Guest, J. K., Topology optimization with linearized buckling criteria in 250 lines of Matlab. Structural and Multidisciplinary Optimization, Vol.63, No.6 (2021), pp.3045-3066.

Gao, X. and Ma, H., Topology optimization of continuum structures under buckling constraints. Computers and Structures., Vol.157, (2015), pp.142-152.

Kanno, Y., Osaki, M., Fujisawa, K. and Kato, N., Topology optimization of trusses with specified buckling load factor using semidefinite programming. Architectural Institute of Japan Structural Papers, Vol.66, No.541 (2001), pp.113-119. (in Japanese)

Kishimoto, N., Noguchi, Y., Sato, Y., Izui, K., Yamada, T. and Nishiwaki, S., Topology optimization for multiple materials based on the level set method. Proceedings of the Japan Society of Mechanical Engineers, Vol.83, No.849 (2017), DOI: 10.1299/transjsme.17-00069.

Li, H., Yamada, T., Jolivet, P., Furuta, K., Kondoh, T., Izui, K. and Nishiwaki, S., Full-scale 3D structural topology optimization using adaptive mesh refinement based on the level-set method. Finite Elements in Analysis and Design, Vol.194, (2021), pp.103561.

Neves, M. M., Sigmund, O. and Bendsøe, M. P., Topology optimization of periodic microstructures with a penalization of highly localized buckling modes. International Journal for Numerical Methods in Engineering, Vol.54, No.6 (2002), pp.809-834.

Neves, M., Rodrigues, H. and Guedes, J. M., Generalized topology design of structures with a buckling load criterion. Structural optimization, Vol.10, No.2 (1995), pp.71-78.

Nishiwaki, S., Izui, K., Kikuchi, N., Topology Optimization(Computational Mechanics Lecture Course)(2013), pp.1-2, Maruzen Publishing (in Japanese)

Shibata, T., Ohtani, R., Komai, K. and Inoue, T., Basics of strength of materials(1991), Baifukan (in Japanese)

Takezawa, A., Nishiwaki, S., and Kitamura, M., Shape and topology optimization based on the phase field method and sensitivity analysis. Journal of Computational Physics,Vol. 229, No.7 (2010), pp.2697-2718.

Vanderplaats, Garret N., Structural optimization-past, present, and future. AIAA Journal, Vol.20, No.7 (1982), pp.992-1000.

Wang, M. Y., and Zhou, S., Phase field: a variational method for structural topology optimization. Computer Modeling in Engineering and Sciences, Vol.6, No.6 (2004), pp.547.

Wang, M. Y., Wang, X., and Guo, D., A level set method for structural topology optimization. Computer Methods in

Applied Mechanics and Engineering, Vol.192, No.1-2 (2003), pp.227-246.

Washidu, K., Finite Element Method Handbook II Application(1983), Chapter3, Baifukan (in Japanese)

Watanabe, K., Formulation of finite elements of geometric nonlinear problems,The University of Tokyo, Special Lecture on Nonlinear Finite Element Method, 6th Lecture Material (2005), pp.54-73 (in Japanese)

Yamada, T., Manabe, M., Izui, K., and Nishiwaki, S., A topology optimization method for geometrically nonlinear problems incorporating level set boundary expressions and a particle method.Journal of Advanced Mechanical Design, Systems, and Manufacturing, Vol.7, No.4 (2013), pp.630-643.

Yamada, T., Izui, K., Nishiwaki, S., and Takezawa, A., A topology optimization method based on the level set method incorporating a fictitious interface energy. Computer Methods in Applied Mechanics and Engineering, Vol.199, No.45-48 (2010), pp.2876-2891.

Yamada, T., Izui, K., Nishiwaki, S., Sato, M. and Tabata, O., Optimal structural design method for capacitive ultrasonic transducers: Topology optimization with equal cross-section shape constraints based on level set method. Proceedings of the Japan Society of Mechanical Engineers, Series A, Vol.76, No.771 (2010), pp.1403-1411. (in Japanese)

Yi, B., Zhou, Y., Yoon, G. H. and Saitou, K., Topology optimization of functionally-graded lattice structures with buckling constraints. Computer Methods in Applied Mechanics and Engineering, Vol.354, (2019), pp.593-619.

Zienkiewicz, O.C., Taylor R.L., The Finite Element Method Volume2 Solid Mechanics(2000), pp.174, Butterworth Heinemann